Electrical Characterization and Modelling of an Ultrasound-Powered Triboeletric Generator for Implantable Applications

Thomas Baudin, Armine Karami, Dabin Kim, Sera Jeon, Dimitri Galayko, Jean-Marc Laheurte, Sang-Woo Kim, Philippe Basset

ELECTRICAL CHARACTERIZATION AND MODELLING OF AN ULTRASOUND-POWERED TRIBOELETRIC GENERATOR FOR IMPLANTABLE APPLICATIONS

Thomas Baudin[1], Armine Karami[1], Dabin Kim[2], Sera Jeon[2], Dimitri Galayko[3], Jean-Marc Laheurte[1], Sang-Woo Kim[2] and Philippe Basset[1]

[1]Univ. Gustave Eiffel, CNRS, ESYCOM, F-77454 Marne-la-Vallée, France,
[2]Energy Harvesting Lab, Yonsei University, Seoul, SOUTH KOREA, and
[3]Sorbonne Université, CNRS, LIP6, F-75005 Paris, FRANCE

ABSTRACT

This paper reports on a method of exhaustive electrical characterization for biocompatible triboelectric nanogenerator (TENG) powered by ultrasound (US). The method is applied to a device made by stacking a 3×3 cm² copper electrode and a dielectric layer made of polyether ether ketone (PEEK). The device is submitted to 20 kHz US illumination, through a medium of medical US gel. Using a synchronous detection technique, the dynamic capacitance variation of the device is measured. The short-circuit current of the device is also measured in the same conditions. The impact of the gap variation between the probe and the dielectric layer on the electrical model is investigated. We use the results to fit an electrical dipole model of the US-driven TENG, which consists in the series connection of a variable capacitance C_t with a DC voltage source V_{TE}. At a fixed 5 mm gap, the mean of C_t was measured as 260.1 pF, and its amplitude as 9.8 pF. We also estimated $V_{TE} = 82$ V from these measurements. The power versus resistive loading is also measured, and is compatible with the electrical model which predicts an optimal loading of 23.8 kΩ. The corresponding power is measured as 0.83 µW. The accurate electrical modeling method reported in this work will enable the design of battery-less implantable medical devices (IMDs) powered by US-driven TENG.

KEYWORDS

TENG, implantable device, ultrasound WPT, kinetic energy harvester.

INTRODUCTION

Triboelectric nanogenerators (TENGs) are electromechanical transducers taking advantage of the combined effect of contact electrification and electrostatic induction to convert energy. They are usually made of two electrodes, one (sometimes both) being covered by a layer of dielectric material. This material is chosen such that it can exhibit uncompensated charges on its surface, through contact electrification with the other electrode. This provides the polarization required for electrostatic induction. Among other numerous applications, TENGs are increasingly considered for powering implantable medical devices (IMDs) thanks to their small size, flexibility, and possibility to be made of biocompatible materials [1]. These applications divide into two families: (i) harvesting the body's internal or environmental kinetic energy, or (ii) by being driven by an external acoustic probe for wireless power transfer (WPT).

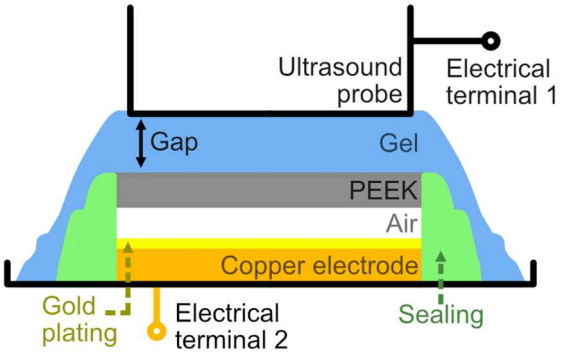

Figure 1: Schematic of the device

Previous studies on this latter application of TENG have already demonstrated the use of ultrasound (US) for effective power transfer to TENG devices through biological tissues [2] as well as the acoustic properties of US-driven TENG [3]. However, the electrical modeling and characterization aspects of US-driven TENGs is overlooked as of now. Specifically, the relative importance between the contact electrification phenomenon and the TENG capacitance variation in the generated signal output has not been studied. Knowing if there is a predominance between these effects will lead to the determination of an electrical model.

In this work, we report on a method for the electrical characterization and modeling of US-TENGs. Our method includes the measurement of the device's dynamic capacitance. This measurement is often neglected in experiments with TENGs and has not been done before for US-TENGs. It is however an important determinant of the device performance, separately from the contact electrification-induced polarization. The method also features classical measurements: short-circuit current and power generated on resistors of several resistance values. We apply the method to a device of 9 cm² made by stacking a polyether ether ketone (PEEK) dielectric layer with a gold-platted electrode, actuated by a 20 kHz ultrasound excitation. By combining the results of these several measurements, we fit an electrical lumped-parameter model of the US-TENG under ultrasound excitation, for different US probe-device distances. Thanks to these results, we show that the capacitance variation is the main driver of the current in steady-state operation.

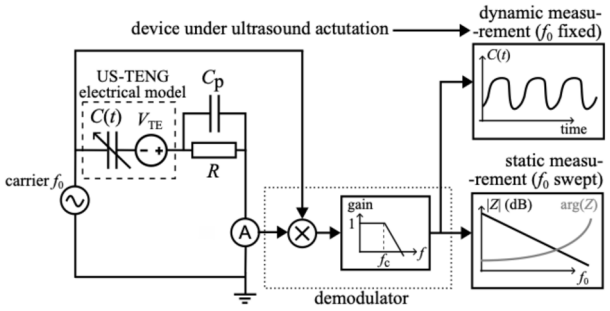

Figure 2: Setup for the static impedance measurement and the dynamic capacitance measurement.

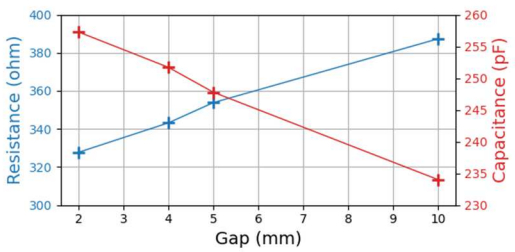

Figure 3: Device 1, static measurement results. The plot shows the variation of the series resistance and capacitance with respect to the probe-device gap.

DEVICE DESCRIPTION

A schematic of the US-TENG device that was fabricated for this study is depicted in Fig. 1. It is made by stacking two layers of $S = 3 \times 3$ cm^2: one of PEEK, and one of gold-platted copper. The two layers are separated by a thin, irregular air gap layer due to their incomplete adhesion. The estimated relative permittivity of the PEEK is $\varepsilon_{\mathrm{PEEK}} = 3.30$.

EXPERIMENTS

Setup and methods

For dynamic measurements, each tested device is stimulated by a custom-made US probe working at 20 kHz frequency and 0.5 W.cm^{-2} power output, of surface comparable to that of the device. The probe is plunged into an ultrasound gel to convey the vibration to the transducer, as depicted in Fig. 1.

The time-varying acoustic pressure resulting from the ultrasound probe excitation makes the PEEK membrane vibrate causing its deformation. This deformation induces a contact between the PEEK layer contact and the bottom gold electrode, at spots distributed throughout its surface. This results in contact-electrification at the PEEK surface. This deformation also induces a periodic variation of the device's capacitance between the conductive element above the PEEK layer – here, the metal US probe through the gel – and the conductive element at the bottom – here, the gold-platted copper electrode. These two effects result in a current being generated through the circuit the device is connected to. Two separate electrical setups are used depending on the conducted experiment.

For the measurement of short circuit current or power on resistors, the device is connected in series to the current input of a *Zurich Instruments MFLI* lock-in amplifier, whose demodulators characteristics are set to measure signals from DC to 100 kHz. Therefore, the apparatus is assimilable to a current amplifier with bandwidth 100 kHz used as an ammeter. The power $P(R)$ on resistance R is then measured as $P(R) = \frac{1}{nT}\int I^2(t)R\,\mathrm{d}t$ where I denotes the measured current, T is the period of the US, and the integration is done on $n = 10$ such periods.

For the measurement of the static impedance or of the dynamic capacitance variation of the device, the setup is depicted in Fig. 2. For each tested value of the gap between the probe and the device, the following procedure is followed. The oscillator output of the lock-in amplifier is set in series with the device and with the current input (a current amplifier). The oscillator feeds the device with AC voltage of amplitude $V_0 = 1$ V and of frequency f_0.

For static measurements, the probe is left inactive: no US excitation is generated. The oscillator frequency f_0 is swept in the range $[1\ \mathrm{kHz}\,;5\ \mathrm{MHz}]$. The phase and amplitude of the subsequently generated current yields the complex impedance $Z(f_0)$ of the device in static conditions. This impedance is then fitted to various basic networks using a least-square criterion, and ultimately the best fitting network is kept, here a series RC_t network. Following the extensive body of work on the modeling of charged dielectrics in TENGs [4], we add to this hypothesized model a DC source of value V_{TE}. This completes the electrical model of the device, ultimately yielding the dipole model in the dashed box of Fig. 2.

For dynamic capacitance measurements, the same setup (Fig. 2) is used. For each probe-device gap, the generated current is amplitude- and phase-modulated by the capacitance variation of the device. From this, the average and amplitude of $C_\mathrm{t}(t)$ are found from $C_t(t) = I_0/(2\pi f_0\sqrt{V_0^2 - I_0^2R^2})$, where I_0 denotes the amplitude of the current demodulated through a 4$^{\mathrm{th}}$ order low-pass filter of cutoff frequency $f_c = 100$ kHz, and R is the resistance value obtained in the static measurement for the corresponding gap.

In total, three different devices had to be used due to the limited lifetime of their sealing under US illumination. In the following, these are referred to Device 1, 2, or 3. The qualitative characteristics of the three devices are expected to be similar, as the results below show. However, there is an inevitable dispersion in the quantitative parameter values, that we can attribute to the lack of precise control of the device building process.

Results

The results of static measurement are depicted in Fig. 3, for Device 1. It can be observed that the device average capacitance $\langle C_\mathrm{t}\rangle$ is a linearly decreasing function of the gap, while the resistance is an increasing value of it.

The evolution of these values following the gap variation is given Fig. 3. We see an increasing resistance and a decreasing capacitance while the gap increases. The non-constant capacitance and resistance may come from the resistivity of the medium between the US-probe and the PEEK layer and a parallel capacitance between the metallic probe and the gold electrode.

From the physical parameters of the device, we can estimate its theoretical capacitance. A global physical

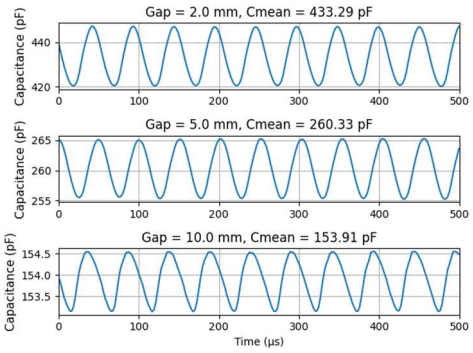

Figure 4: Device 2, dynamic device capacitance measured through synchronous detection under ultrasound excitation for selected probe-device gaps.

approach of TENG was given in [5]. It shows that the total capacitance is equivalent to two capacitors in series.

$$C_{TENG} = \frac{C_{die}C_{var}}{C_{die} + C_{var}} = \frac{S}{\frac{d_{die}}{\varepsilon_{die}} + \frac{d_{var}}{\varepsilon_{var}}} \quad (1)$$

with C_{TENG} being the global capacitance of the device, C_{die}, C_{var} are the capacitance of the dielectric and the air layer, respectively. It is then expressed with the facing surface S and the value of permittivity ε and thickness d for each layer. Here the PEEK layer has a thickness of 50 µm with a relative permittivity of 3.30, and the air gap can be estimate within 0 and 50µm giving a framing of capacitance C_{TENG} between 526 pF and 122 pF. The measured mean capacitance of the device is always in between these values.

The results of the dynamic capacitance measurements are shown in Fig. 4. These measurements were carried out in device 2. We observe almost-sinusoidal waves of 50 µs period, corresponding to the 20 kHz ultrasound base frequency, with different amplitude and mean value depending on the gap distance. Similarly, the current was directly measured without synchronous detection, and the results are shown in Fig. 5. There, higher harmonics seem to have stronger impact on the current variation.

Before these measurements, the degradation of the Device 1 caused the failure of the sealing part of the device. Gel could then infiltrate into the air gap and highly mitigate the capacitance variation and the contact electrification effect between the PEEK layer and the electrode because of the increase in humidity, thus diminishing the performance of the transducer. Hence, the next dynamic measurement was made using a different, but similar with first, device hereafter named Device 2.

In these measurements, we see a highly variating average capacitance, compared to the static measurement of Device 1. Both these measurements were used to extract and compare the variation amplitude (in capacitance and current) with respect to the gap (Fig. 6). We can see a correlation between the two amplitudes meaning that the current generated by the TENG depends on its capacitance amplitude variation.

We measured the power across resistor using a third device, Device 3, again similar to the two precedent ones. From the measurement of the current through different resistor value, we can evaluate the absorbed power (Fig. 7).

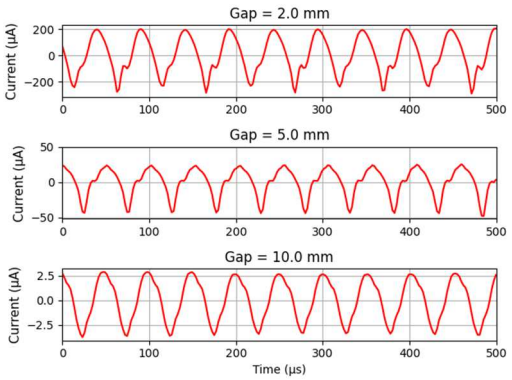

Figure 5: Device 2, short-circuit measurements under ultrasound excitation for selected probe-device gaps.

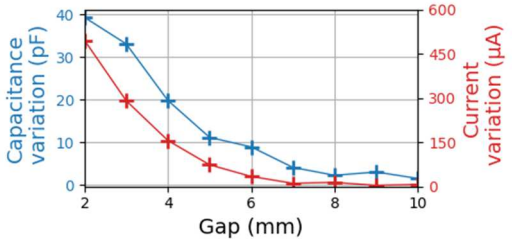

Figure 6: Device 2, measured capacitance variation amplitude and short-circuit current amplitude vs. the gap between the US probe and the PEEK layer.

With the listed resistor, we measured a maximum power of 835 nW at 27 kΩ. The optimal load value was computed to be 23.77 kΩ.

EXTRACTED ELECTRICAL MODEL

From the variation of capacitance and short-circuit current with respect to the gap distance between the US-probe and PEEK layer, we can see that the current amplitude is correlated with the capacitance variation. This correlation is hinting that we can have a DC voltage source in series with a variable capacitor as a model.

Moreover, the frequency sweep measurement indicates a static model of the setup like a RC series circuit. From this model, we start with the equation Eq. 2.

$$\frac{Q(t)}{C_t(t)} + R\dot{Q}(t) = V_{TE} \quad (2)$$

Seeing the previous capacitance variation results, we can say that the variation is weak compared to the mean capacitance value. Thus, with the hypothesis that V_{TE} is constant, the voltage across the capacitor becomes:

$$V_{C_t} = \frac{Q(t)}{C_t(t)} = \frac{Q(t)}{C_0 + c_t(t)} = \frac{Q_0 + q(t)}{{C_0}^2}\left(C_0 - c_t(t)\right) \quad (3)$$

The terms $q(t)$ and $c_t(t)$ are the small variation of charges and capacitance, respectively. C_0 and Q_0 are the average value of $C(t)$ and $Q(t)$. After developing Eq. 3,

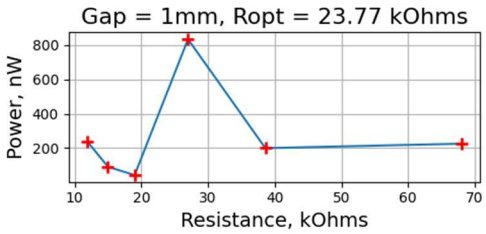

Figure 7: Device 3, power variation with respect to the resistive load value

we keep only the term below the second order of small quantities $c_t(t)$ and $q(t)$. Replacing in Eq. 2, and separating the equation for each order gives:

$$\begin{cases} \dfrac{Q_0}{C_0} = V_{TE} \\ \dfrac{q(t)}{C_0} + R\dot{q}(t) = \dfrac{Q_0}{C_0}\dfrac{c_t(t)}{C_0} \end{cases} \quad (5)$$

We can see that the variable capacitor is equivalent to a fixed capacitor C_0 in series with a voltage source of value $V_{TE}\frac{c_t(t)}{C_0}$. Eq. 5 is linear and can be express in the Laplace domain:

$$\frac{q(s)}{C_0} + s \cdot R\, q(s) = V_{TE}\frac{c_t(s)}{C_0} \quad (6)$$

Optimal load resistance

The value R is the series resistance of the full device, taking account for the probe-fluid contact, the gel resistance and the TENG resistance. Eq. 6 can then provide the short-circuit current:

$$i_{sc}(s) = s\, q(s) = V_{TE} \cdot \frac{c_t(s)}{C_0} \cdot \frac{s\, C_0}{1 + s\, RC_0} \quad (7)$$

In the case of a sinusoidal variation of $c_t(t)$ with an amplitude $|c_t|$, the amplitude of the current is:

$$|i_{sc}| = s\, q(s) = V_{TE} \cdot \frac{|c_t|}{C_0} \cdot \frac{\omega\, C_0}{\sqrt{1 + (\omega RC_0)^2}} \quad (8)$$

From this model, we can find the optimal resistance value giving the maximum power output from the device. We complete the Eq. 8 with a series load resistance R_L:

$$|i_{sc}| = V_{TE} \cdot \frac{|c_t|}{C_0} \cdot \frac{\omega\, C_0}{\sqrt{1 + (\omega(R + R_L)C_0)^2}} \quad (9)$$

The power absorbed by the load is finally:

$$P_L = \frac{1}{2}\,|i_{sc}|^2 R_L = \frac{1}{2}\left(V_{TE}\frac{|c_t|}{C_0}\right)^2 \frac{\omega^2 {C_0}^2 R_L}{1 + (\omega(R + R_L)C_0)^2} \quad (10)$$

We can now have the value of R_{opt} which is the value of R_L when $\frac{dP_L}{dR_L} = 0$.

$$R_{opt} = \sqrt{R^2 + \frac{1}{\omega^2 {C_0}^2}} \quad (11)$$

Constant voltage

The constant voltage of the device can also be determined from the short-circuit current amplitude, the capacitance variation amplitude and the average capacitance of the TENG.

$$V_{TE} = \frac{|i_{sc}|\sqrt{1 + (\omega RC_0)^2}}{|c_t|\,\omega} \quad (12)$$

EXTRACTION OF PARAMETERS

From the new model and the measurement results, we can extract the parameters of the device, more precisely $R, C_0, |c_t|, |i_{sc}|, V_{TE}$ and R_{opt}. Here, we've extracted the values for a 5mm gap setup of the Device 2.

Table 1: Device 2, Parameters given for the experimental device with a 5 mm gap between probe and triboelectric layer

R	309 Ω
C_0	260.1 pF
$\|c_t\|$	9.8 pF
$\|i_{sc}\|$	73.6 μA
V_{TE}	82.7 V
R_{opt}	30.6 $k\Omega$

CONCLUSION

The proposed electrical analytic model for the US-TENG is a DC voltage source in series with a variable capacitor and an internal resistance. Reliability of the devices also need to be improved.

The characterized US-TENG can be used in the design of battery-less sensors that can be passively interrogated by actuating the US-TENG as an AC source. Then, the sensor information can be retrieve using a near-field wireless transfer subsystem for reading the information from outside the body. Therefore, this work is in an important step toward the design of a fully implantable US-TENG powered sensing system.

We aim at a possible implantable sensor modulating the US-TENG power input and communicating the sensor's informations through a very low frequency (VLF) near-field wireless subsystem also implanted under the skin.

ACKNOWLEDGEMENTS

The authors acknowledge the support of the French Agence Nationale de la Recherche (ANR) under reference ANR-21-CE05-0032 INTRICATE.

REFERENCES

[1] Xiao, X. et al, *Ultrasound-Driven….* Small Methods, 2023. **7**(6): p. 2201350.

[2] Hinchet, R. et al, *Transcutaneous ultrasound….* Science, 2019. **365**(6452): p. 491.

[3] Deng, W. et al. , *Computational investigation….* Nano Energy, 2022. **91**: p. 106656.

[4] Hinchet, R. et al., *Understanding and modeling….* Nano Energy, 2018. **47**: p. 401-409.

CONTACT

Armine Karami: armine.karami@univ-eiffel.fr